Investigating Dynamic Thermal Behavior of Continuous Casting of Steel with CONOFFLINE

BRYAN PETRUS, ZHELIN CHEN, JOSEPH BENTSMAN, and BRIAN G. THOMAS

A new model, CONOFFLINE, has been developed to simulate transient thermal behavior of a longitudinal section down a continuous steel slab-casting machine. The model was first verified by comparing its predictions of shrinkage through the strand thickness with transient measurements of roll forces in a thick-slab caster during a series of speed changes. The model was then applied to investigate the evolution of temperature and shell thickness in a typical caster after sudden changes in casting speed. Simple equations are proposed to estimate the settling time of metallurgical length and surface temperature during sudden speed changes for both thin- and thick-slab casters. Finally, the influence of different spray cooling control methods on these behaviors during casting speed changes is investigated.

https://doi.org/10.1007/s11663-020-01941-6

I. INTRODUCTION

THE process of continuous casting of steel slabs, shown in Figure 1, is best operated in steady state. The metallurgical length, which defines the region of final solidification, should occur within the roll containment region. Changing casting conditions sometimes extends the liquid core beyond containment, which causes a serious "whale" defect, where the internal ferrostatic pressure causes expensive and dangerous bulging.[1] To lessen centerline defects such as macrosegregation and porosity, the final solidification region should fall within the range of soft-reduction equipment, which is available in many casters to provide extra squeezing of the strand on segregation-sensitive steel grades during this critical time.[2–4] Changing casting speed requires changing the location down the casting machine where soft reduction is required. Spray cooling systems are designed to control the surface temperature of the strand, in order to avoid surface cracks, especially during unbending, where crack-sensitive grades suffer metallurgical embrittlement and transverse cracks, if the surface temperature is in a detrimental temperature range.[5,6] Many operations use a simple spray table to accomplish this task, which works well during steady-state conditions. During a speed change, however, spray cooling should be adjusted dynamically in each spray zone at different times,[5,7] which is more challenging. Sudden drops in casting speed, which often occur due to automated alarm systems designed to detect and avoid sticker breakouts in the mold,[8,9] can lead to internal cracks due to increased thermal stress,[10] and other problems, such as centerline bridging and severe centerline segregation.[8] In fact, most defects in the process arise during transient conditions, especially involving changes in casting speed.[7,8,10–12]

Although steady-state conditions are preferred, casting speed changes arise during operation for many reasons. In addition to the examples just mentioned, casting speed is usually lowered during startups, tailouts, ladle changes, tundish changes, and other operational conditions. Speed changes are also required to accommodate schedule changes, upstream delays in steelmaking, or downstream delays in rolling (for operations with hot charging or thin-slab casting). Because so many defects arise due to these changes, it is important to understand the dynamic thermal behavior of the continuous-casting process during transient conditions. This includes how the strand surface temperature, shell thickness profile, and especially the metallurgical length vary during changes in casting speed, for different types of secondary cooling control.

Experimental investigation of thermal behavior in a continuous caster is difficult because measurements are at best unreliable and at worst impossible, owing to the unreliability of temerature sensor such as optical pyrometers.[9,13] Therefore, computational modeling has been used extensively to understand continuous casting, going back to when the process was new.[14,15] These early models, and the many increasingly sophisticated and detailed models that succeeded them, such as

BRYAN PETRUS is with the Nucor Steel Decatur, 4301 Iverson Blvd, Trinity, AL 35673. ZHELIN CHEN and JOSEPH BENTSMAN are with the University of Illinois at Urbana-Champaign, 1206 W Green St, Urbana, IL, 61801. BRIAN G. THOMAS is with the Colorado School of Mines, 1610 Illinois St, Golden, CO, 80401. Contact e-mail: bgthomas@mines.edu

Manuscript submitted October 14, 2019.
Article published online September 24, 2020.

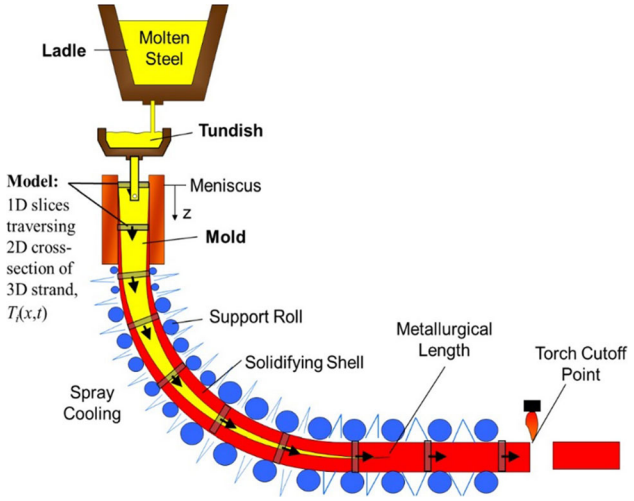

Fig. 1—Overview of continuous casting process.

in References 16, 17, 18 have focused mainly on steady casting when casting conditions are constant. Transient behavior has received much less study, even though it is known to be very important

Previous computational models of transient thermal behavior in continuous casting have focused on slab casting. An early model, DYCOOL, by Louhenkilpi and co-workers,[19] modeled transient heat conduction in a 2-D longitudinal slice through the center plane of the caster using the finite-element method and implicit time stepping. The model was used to simulate a transient case of 40 pct spray flow rate, and good agreement between the calculated and measured surface temperature was obtained. A following model, DYN3D,[20,21] uses steel properties and solid fraction/temperature relationships based on multicomponent phase diagram computations, was validated for copper casters with measurements of liquid pool depth and by mold thermocouple measurements.[21] The DYSCOS model[6] also modeled the 2-D longitudinal domain, using the finite volume method and a tri-diagonal matrix algorithm solver with alternating direction implicit sweeping. Parametric studies were performed using the DYSCOS model to study the relative effects of casting variable changes on the surface temperatures and solidification conditions, and results show that casting speed is the most critical factor affecting thermal and solidification conditions. Ma[22] developed a real-time 2-D model solved by the finite volume method. The model was validated and applied to a dynamic control system to adjust operating parameters. Later, the CONONLINE model[5,23] was developed to model a similar 2-D longitudinal domain, gaining sufficient speed to run in real-time by exploiting time-delayed interpolation of multiple 1-D moving slices. This model has been running online at the Nucor Steel casters in Decatur, AL for more than a decade. CONOFFLINE, an offline version of CONONLINE, has been developed recently to study transient behavior. Chen and co-workers[7] investigated the performance of different spray cooling control methods to maintain constant metallurgical length for a small speed drop from 1.7 to 1.5 m/min of a 220-mm thick caster. Results showed that the ability to control metallurgical length *via* spray flow rates is limited, especially in thicker slabs. They[8] also investigated the transient casting conditions that lead to detrimental centerline bridging that likely leads to porosity and centerline segregation problems. CONOFFLINE has also been used to investigate liquid level fluctuations in the mold due to dynamic bulging of the strand.[12]

In this work, the CONOFFLINE model is used to investigate the thermal behavior of typical continuous steel slab casters during changes in casting speed. First, Section II gives a brief overview of the CONOFFLINE model. Section III then compares CONOFFLINE model predictions with measurements from a trial performed at the ArcelorMittal Burns Harbor steel mill, in order to validate the model.[24] Finally, the CONOFFLINE model is applied to investigate changes in surface temperature and metallurgical length histories for different speed change scenarios, spray control methods, and casters.

II. MODEL DESCRIPTION

CONOFFLINE models the complete temperature distribution, and solidified shell thickness evolution, in a 2-D centerline cross-section through the entire continuous caster of steel slabs, from the meniscus (top surface level in the mold), to beyond the roll containment region at the end of secondary cooling. It is based on the real-time dynamic model CONONLINE.[5] Both models solve the transient heat conduction equation with advection

$$\rho c_{\mathrm{p}}^{*}\left(\frac{\partial T}{\partial t}+v_{\mathrm{c}}\frac{\partial T}{\partial z}\right)=\frac{\partial}{\partial x}\left(k\frac{\partial T}{\partial x}\right)+\frac{\partial}{\partial z}\left(k\frac{\partial T}{\partial z}\right) \quad [1]$$

where $T(x,y,z,t)$ is the temperature at any given point in a material and v_{c} is the casting speed. The density ρ, thermal conductivity k, and effective specific heat c_{p}^{*} are temperature-dependent thermal properties of the given steel alloy. The effect of solidification is incorporated by adjusting the effective specific heat, to include the latent heat of solidification

$$c_{\mathrm{p}}^{*}=c_{\mathrm{p}}+L_{\mathrm{f}}\frac{\mathrm{d}f_{\mathrm{s}}}{\mathrm{d}t} \quad [2]$$

where c_{p} is the specific heat, L_{f} is the latent heat of solidification, and f_{s} is the fraction of the steel that is solid at a given temperature. In this work, z is in the casting direction, and x is in the slab thickness direction, (smaller of the two cross-sectional dimensions). Note that the heat conduction in the y-direction, the width direction (larger of the cross-sectional dimensions), can be neglected, owing to the large aspect ratio of the cross-section. The origin is at the center of the strand and at the meniscus of the caster. Phase fractions during solidification were found using a simple micro-segregation model.[25] Typically a solid fraction

of 70 pct is considered enough to resist whale formation,[13] and is used in this work to define shell thickness and metallurgical length.

The top surface boundary condition, defined at the meniscus ($z = 0$), is to fix the steel at the pouring temperature, T_{pour}. Thus, the effects of turbulent fluid flow in the liquid pool are neglected in this model. At the steel surface ($x = \pm L/2$), heat is removed by heat flux across the interfacial gap while in the mold, and by natural convection, radiation, convection to the spray water hitting the surface, and conduction contact to the containment rolls while in the secondary cooling region. A summary of these boundary conditions is given below, with more detail provided elsewhere.[5]

Heat flux in the mold depends on many complex phenomena. CONONLINE adopts a heat flux profile that is calibrated in real-time to match the average heat flux in the mold based on the current measurements of temperature increase and flow rate of the mold cooling water as explained in Reference 26. In this work using CONOFFLINE, the average mold heat flux is calculated as an empirical function of casting speed for the given casters, which are given later.

Heat flux due to the water sprays in secondary cooling are based on the empirical correlation of Nozaki,[27] in which

$$\begin{aligned} q_{sw} &= h_{sw}(T_{surf} - T_{sw}) \\ &= 0.3925 \cdot Q_{sw}^{0.55} \cdot (1 - 0.0075 \cdot T_{sw})(T_{surf} - T_{sw}) \end{aligned} \quad [3]$$

where T_{surf} is the surface temperature of the steel (K), T_{sw} is the spray water temperature (K), and Q_{sw} is the rate (L/m^2/s) of the spray water flux hitting the steel surface at that point along the caster. Heat flux due to rolls is set to be a fraction of the total other heat removals at the surface. The specific fraction, f_{roll}, is a calibration parameter and may be different for each spray zone (in this work, f_{roll} is set to 0.25 for all spray zones). Natural convection is treated as a constant 8.7 W/m^{2}K.

Solving the nonlinear partial differential Eq. [1] with sufficient mesh resolution to achieve reasonable accuracy is computationally expensive, but fortunately, the model can be simplified, as explained in the next section.

A. *Solution Methodology*

This transient heat conduction problem in a 2-D Eulerian (laboratory-based) frame of reference, Eq. [1], is solved here by first transforming it into a series of 1-D transient moving-slice problems in a Lagrangian (material-based) frame of reference. This is possible because heat conduction in the axial (casting) direction, z, is small. This can be demonstrated by examining the Péclet number, which is the ratio of advection to conduction heat transfer rates in the z-direction,

$$\mathrm{Pe} = \frac{v_c L_z \rho c_p}{k} \quad [4]$$

where L_z is the characteristic length in the casting direction. For example of the ArcelorMittal Burns Harbor CC1 caster,[24] taking L_z to be the caster length(30 m), casting speed v_c to be 1 m/min, density ρ to be 7400 kg/m^3, thermal conductivity k to be 30 W/mK, and specific heat c_p to be 670 J/kgK, then the Péclet number is 9073. So conduction in the shell in the z-direction is negligible relative to advection in the z-direction due to the casting speed. The characteristic length in the x-direction, L_x, half the thickness of the slab (0.13 m), is much smaller than L_z. This means that the temperature distribution is governed by conduction in the x-direction and advection in the z-direction. Further taking a series of slices through the slab thickness which move with the steel in the z-direction at the casting speed in a Lagrangian reference frame as the simulation domain, Eq. [1] simplifies to

$$\rho c_p^* \frac{\partial T}{\partial t} = \frac{\partial}{\partial x}\left(k \frac{\partial T}{\partial x}\right) \quad [5]$$

Note that in regions of high axial temperature gradient, such as near the strand surface where a roll contacts the strand, Pe becomes much smaller, axial conduction becomes more significant, and local temperature may be less accurate with this simplification.

B. *2-D Eulerian Frame Model by Delay Interpolation*

The series of 1-D slice models, given by Eq. [5] can be solved very efficiently, but it only gives the temperature at the location of the moving reference frame, which in turn depends on the casting speed history. The 2-D Eulerian model solution can be constructed from the 1-D Lagrangian models to produce the temperature and shell thickness profile along the entire caster (z) and through its thickness (x) in time (t) using delay interpolation. The CONOFFLINE model manages the simulation of N different moving slices starting at the meniscus at different times to achieve a fixed z-distance spacing in-between. Figure 1 shows an illustration example with $N = 10$. CONOFFLINE updates the temperature estimate $\hat{T}(x, z, t)$ every Δt seconds. During each time interval, CONOFFLINE tracks the temperature and shell thickness evolution in each slice over this interval, given the previously calculated and stored temperature distribution across the thickness of that slice at the start of the interval.

Denote $T_i(x, t)$ as the solution to Eq. [5] for the ith slice, starting at the meniscus at time t_i^0. This would give an "exact estimate" (meaning only with modeling and numerical error) of the temperature for

$$\hat{T}(x, z_i(t), t) = T_i(x, t) \quad [6]$$

where

$$z_i(t) = \int_{t_i^0}^{t} v_c \, dt. \quad [7]$$

In order to get temperature estimation $\hat{T}(x, z, t)$ for locations in-between the slices, $z_{i-1} < z < z_i$, CONOFFLINE uses "delay interpolation",[5] substituting the most recent "exact estimate" of the temperature at that location, *i.e.*, the temperature of the most recent slice to pass through that location. The "delay interpolation method" can be thought of as a version of the "sample and hold" interpolation method in the conversion of discrete measurements to analog signals,[28] which assumes the values of the data in-between samples are constant at the most recent measurements. In the case of CONOFFLINE, the slice prediction is the "measurement" and the CONOFFLINE output at any point in the caster updates when a slice passes and is constant otherwise.

The approximation error introduced is a function of the extent of transient effects in the laboratory frame and slice spacing.[5] This error is most substantial when the casting speed is small, increasing the residence time of the slices in the caster, or when the casting conditions change drastically in a small amount of time. Figure 2 shows this error under a worst-case scenario, a sudden drastic casting speed drop. In this figure, slices 1, 2, and 3 are consecutively created slices. Slice 2 and 3 are at location z_2 and z_3 at the time when the data is collected. Through the "delay interpolation method",[5] CONOFFLINE takes the temperature and shell thickness from the history of slice 3 before z_3, the history of slice 2 between z_2 and z_3, and the history of slice 1 after z_2. Due to the drastic speed drop, slice 3 is much colder than slice 2, which is much colder than slice 1. This leads to jumps in temperature and shell thickness at the points where CONOFFLINE switches from an older slice to a newer one.

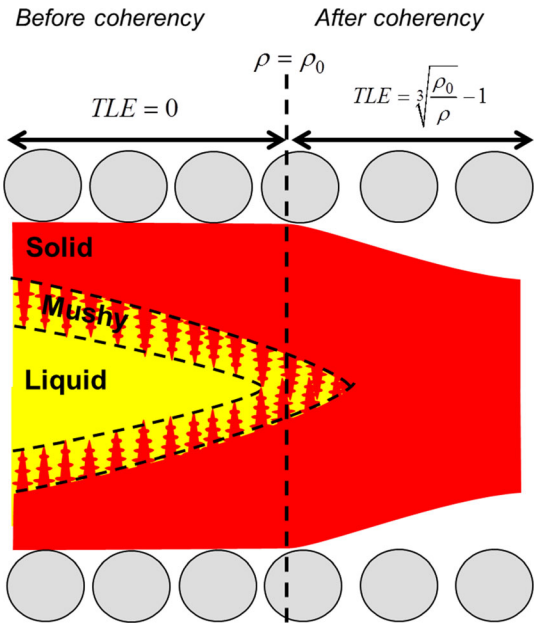

Fig. 3—Illustration of simple thermal shrinkage prediction method used in CONOFFLINE.

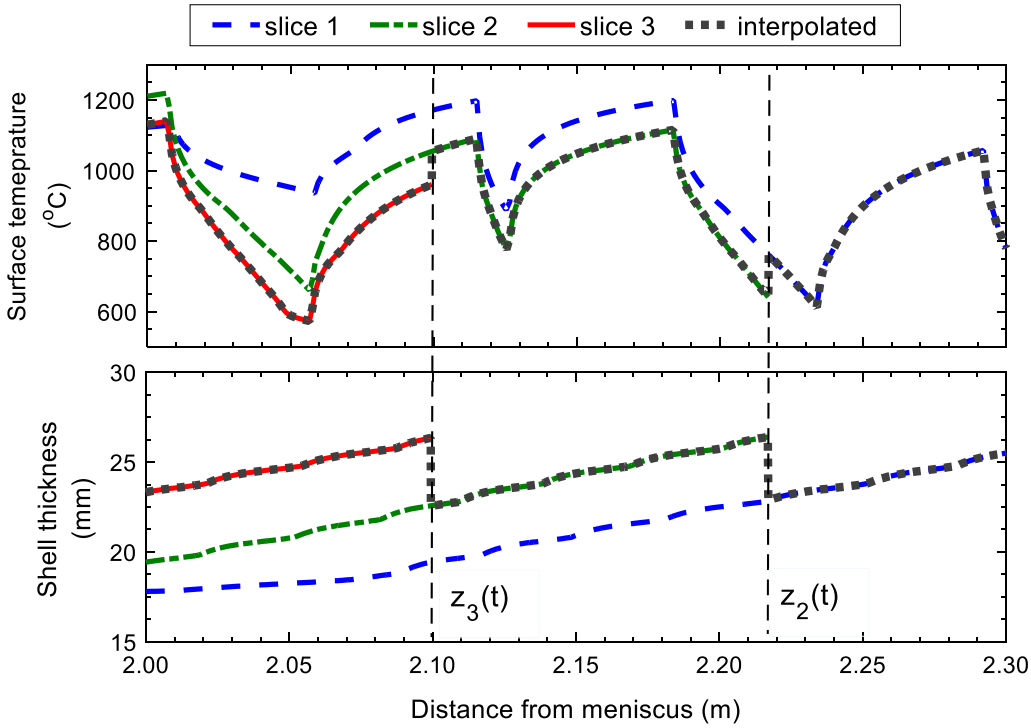

Fig. 2—Example surface temperature and shell thickness profile histories for three consecutive slices, and delay-interpolated profiles from CONOFFLINE.

C. *Thermal Shrinkage Model*

The strand thickness, L, is estimated from the 2-D thermal history solution described above by applying a thermal shrinkage model. As shown in Figure 3, ferrostatic pressure in the liquid tends to push the strand outward anywhere that is not fully solidified. In these locations down the caster, the width of the strand matches the roll gap. Elsewhere, after the strand is fully solid, the steel shrinks according to its temperature and natural thermal contraction. To predict the average shrinkage of the strand thickness, as a post-processing step, the thermal linear expansion (TLE) function based on previous measurements[29–31] is used. For a material of length L, the TLE is the relative change in thickness from the strand thickness at the reference temperature, T_{ref}, where TLE is chosen to be 0:

$$\text{TLE}(T) = \frac{\Delta L(T)}{L(T_{\text{ref}})} = \frac{L(T) - L(T_{\text{ref}})}{L(T_{\text{ref}})} \quad [8]$$

TLE is calculated from the weighted average of the density of the individual phases, $\rho(T)$, as follows:

$$\text{TLE}(T) = \sqrt[3]{\frac{\rho_{\text{ref}}}{\rho(T)}} - 1 \quad [9]$$

Temperature-dependent functions[18] are used to calculate the thermal properties for a low-carbon (0.05 wt pct C) steel and are given in Figure 4, in which the reference temperature is chosen to be the liquidus temperature. The following fast and simple methodology to estimate strand shrinkage is implemented into CONOFFLINE as follows:

1. Calculate temperature, $T(x, z)$, and phase fractions, $f_s(x, z)$, everywhere in the strand.
2. Using the density models,[30] the average nominal density over the cross-section, $\rho(z)$, is calculated as a function of the temperatures, phase fractions, and steel composition.

$$\rho(z) = \frac{1}{L}\int_0^L \rho(T(x, z))\mathrm{d}x \quad [10]$$

3. Assuming the material is coherent for a solid fraction $f_s \geq f_{s,\text{cohere}}$, find the point of coherency. *i.e.*, position z_{cohere} such that $f_s(x, z) \geq f_{s,\text{coherent}}$ for $z \geq z_{\text{cohere}}$. For $z < z_{\text{cohere}}$, the ferrostatic pressure pushes the strand out to the containment rolls. After z_{cohere}, normal thermal shrinkage applies. Hence, the density at z_{cohere} is used as the reference density for the shrinkage calculation.
4. Calculate the thermal linear expansion TLE(z),

$$\text{TLE}(z) = \begin{cases} 0, & z < z_{\text{cohere}} \\ \sqrt[3]{\frac{\rho(z_{\text{cohere}})}{\rho(z)}} - 1, & z \geq z_{\text{cohere}} \end{cases} \quad [11]$$

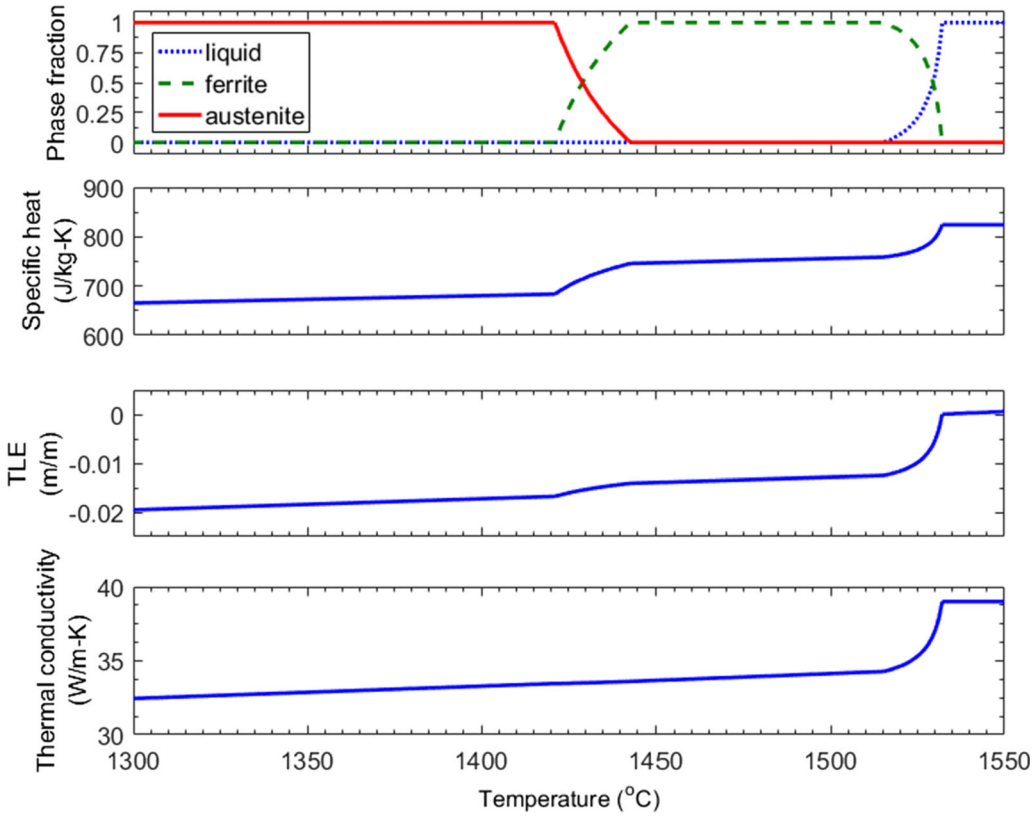

Fig. 4—Properties of 0.05 wt pct Carbon steel. Reprinted with permission from Ref. [9].

III. MODEL VALIDATION

To investigate the transient change in metallurgical length during casting speed changes, CONOFFLINE was applied to the ArcelorMittal 260 mm thick slab caster at the Burns Harbor CC1 caster[24] where measurements during transient conditions were made during trials to redesign the roll gap. Strain gauges were installed on some of the support rolls to measure the changing forces exerted on those rolls by the strand.[24] Figure 14 in that paper illustrates those measurements, and they are reproduced here and used for validation of the CONOFFLINE model.

The roll force measurements collected by the strain gauges during the ArcelorMittal plant trial[24] change according to the decrease and increase in cast speed. These changes are caused by the changing location of the liquid core. While there is still liquid beneath a given support roll, the ferrostatic pressure of the liquid pushes the shell against the roll, causing high roll load measurements. When the strand is solid beneath the support roll, there is no ferrostatic pressure and the measured roll loads are smaller, according to the shrinkage of the strand thickness. Thus, the shrinkage of the shell cross-section, predicted by CONOFFLINE from the simulated temperature and shell thickness distribution as described in the previous section, can be used as a relative indication of the roll force.

A. *Casting Conditions*

Most of the casting conditions for the chosen trial, including caster geometry, roll pitch profiles, and casting speed histories were taken from Reference 24. The trial involved a typical low-carbon steel grade, so properties and pour temperature for 0.05 wt pct C steel, given in Table I and Figure 4, were assumed. The roll gap profile was taken from measurements prior to casting when the machine was cold, although the authors note that the gap expanded when steel was in the caster. The boundary heat fluxes in the mold and spray zones were estimated from previous experience, as described below, and then calibrated to match the reported metallurgical lengths measured at steady state for two different casting speeds. There are no adjustable parameters in the CONOFFLINE model for transient conditions.

For simplicity, boundary heat flux is assumed to be the same on either side of the strand. In the mold, average heat flux was based on an empirical correlation with casting speed for a thin-slab caster,[26] as follows:

$$\bar{q}_m\left[\mathrm{MW/m^2}\right] = 0.9535(v_c[\mathrm{m/min}])^{0.5} \qquad [12]$$

Table I. Steel Properties Used in All Simulations

Steel Property	Value
Liquidus Temperature	1532.1 °C
Solidus Temperature	1515.3 °C
Pour Temperature	1550 °C
Latent Heat of Solidification	271 kJ/kg

The exponent of 0.5 is the theoretical value for constant surface temperature in the mold,[32] and is close to that reported previously.[26,33] This average mold heat flux was converted into a heat flux profile as described elsewhere.[5]

In secondary cooling, heat flux was assumed to depend on the water flux impacting the steel surface, according to relations given in previous work.[5,7,18,27] The water flow flux was assumed to vary linearly with casting speed according to

$$Q_{sw}\left[\mathrm{L/m^2/min}\right] = -160 + 600 v_c[\mathrm{m/min}] \qquad [13]$$

All sprays were assumed to cover a length of 30 mm in the z-direction.

The three constants in Eqs. [12] and [13] were chosen to match the reported metallurgical lengths[24] at two steady-state casting speeds: 28 m at 1.1 m/min and 23 m at 0.9 m/min, and are consistent with previous work.[26] It is important to emphasize that there are no adjustable parameters in the model for transient conditions. These two speeds roughly approximate the 0.762 to 1.143 m/min speed range of the dynamic trial. Obviously, these assumptions become increasingly unrealistic for speeds outside of the calibrated range, and the variations caused by separate heat extraction to the rolls and by different nozzle configurations in different spray zones are ignored. Therefore, the model-predicted surface temperatures are not expected to be accurate. However, because the metallurgical lengths were calibrated to be accurate, the overall heat flux profiles are expected to be reasonable, so the model predictions of shell thickness and internal temperature are expected to roughly match those at the plant.

More importantly, the dynamic behavior incorporated into the model *via* the 2-D transient heat conduction equation is expected to be accurate. Furthermore, this test case also serves as validation of the CONOFFLINE solution method of a series of 1-D slices *via* Eq. [5].

B. *Steady-State Simulation Results*

As mentioned above, model calibration was performed by choosing the three constants in the mold heat removal and secondary cooling water spray rate equations to match reported metallurgical lengths in the plant trial.[24] Figures 5 and 6 display some of the simulation results at a steady casting speed of 1.1 m/min, which had a metallurgical length of 28 m. Figure 5 shows temperature profiles through the thickness at four locations down the caster. In this figure, 0 mm on the x-axis is the inner radius surface and 259 mm is the outer radius surface. Figure 6 shows the corresponding results down the length of the entire caster from the meniscus to the last containment roll.

The middle graph in Figure 6 illustrates that final solidification actually occurs over a range, specifically from 25.4 to 28.2 m. Steel, being an alloy, solidifies over the temperature range from liquidus to solidus. In this range, the centerline consists of dendrites and interdendritic liquid, which is often called the "mushy zone."

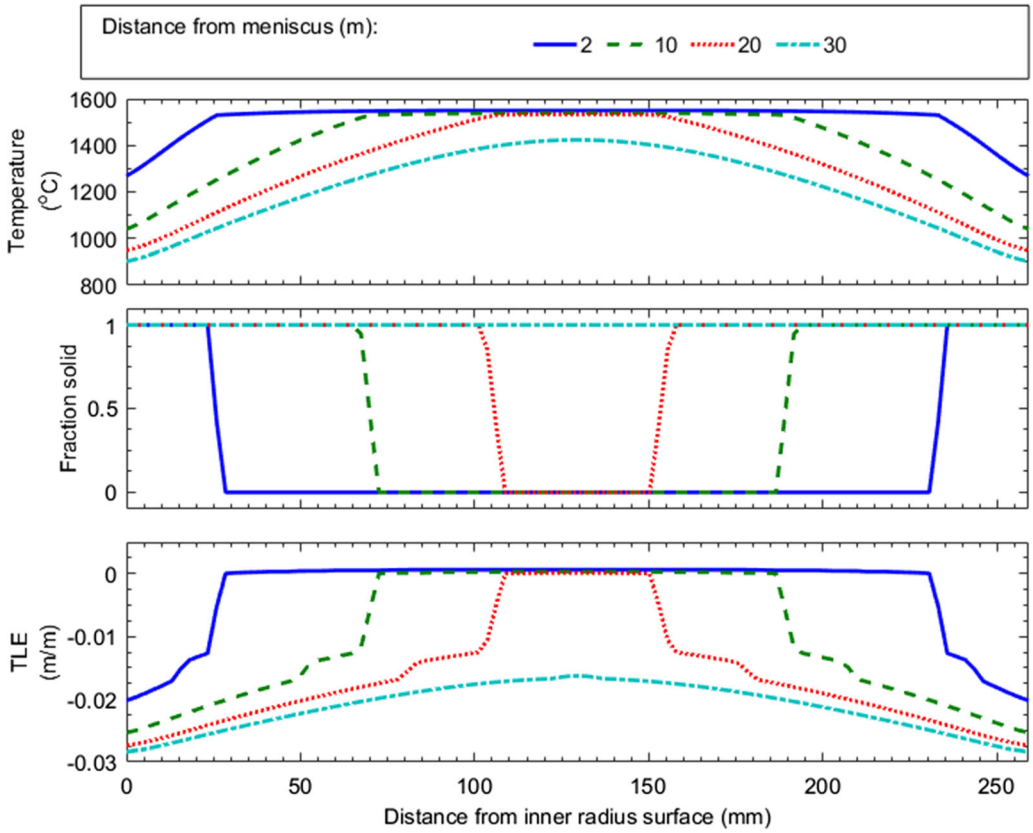

Fig. 5—Steady-state temperature, solid fraction, and TLE profiles through a transverse slice of the strand at different times/distances down the caster, (AM caster at 1.1 m/min).

Although different definitions are possible, the "metallurgical length" of primary interest in this work is when the dendrites growing from opposite sides of the strand weld together sufficiently to provide enough coherency to prevent the ferrostatic force from the liquid pool from pushing the strand against the containment rolls, leading to a drop in roll force. In previous work,[5,13] a solid fraction of 0.7 was found to match reasonably well with predicting this metallurgical length, which in this case gives 27.8 m, as shown in Figure 6.

The bottom graph in Figure 5 illustrates that a large amount of thermal shrinkage occurs near the metallurgical length, when the molten steel solidifies from liquid to delta-ferrite. Even more shrinkage occurs just after the strand becomes fully solid. This is also seen at the end of the bottom graph in Figure 6. This is due to the faster cooling that is possible when there is no more liquid to supply latent heat. Of course, the extent of the shrinkage also depends on the steel grade, which affects the shrinkage from delta-ferrite to austenite, and the spray cooling conditions.

C. *Thermal Shrinkage and Machine Taper*

The plant trial[24] reports improved slab centerline quality when the machine taper is set at 0.34 mm/m. It is well known that centerline quality is best when machine taper approximately matches the natural shrinkage of the steel during final solidification,[34] which provides a possibility for quantitative comparison with the model TLE prediction. Prior to final solidification, the predicted TLE (solid blue line) contrasts with the dotted green line in Figure 6, which represents the strand thickness without consideration of machine taper. This is illustrated qualitatively in Figure 3. Both of the predicted TLE lines then shrink from -0.02013 m/m when coherency is reached (27.77 m) to -0.02138 mm/m at the end of the caster (30m), Converting these numbers to an average slope, the predicted ideal machine taper in the critical range near final solidification is 0.145 mm/m. This is less than the reported machine taper by more than a factor of 2.

However, the TLE equation [11] assumes isotropic behavior, so there is equal thermal shrinkage in all directions. In the continuous casting strand, results from a thermal-mechanical model[17] have shown that the strand shrinks more in the thickness direction, because the axial (casting) and width directions are more strongly constrained. This shows that the simple shrinkage prediction of this model behaves as expected and should produce reasonable qualitative behavior.

D. *Transient Simulation Results*

Figures 7(a) and (b) show casting speed and strain gauge measurements collected from the ArcelorMittal plant trial.[24] The casting speed initially drops, which should lead to a smaller metallurgical length. After a

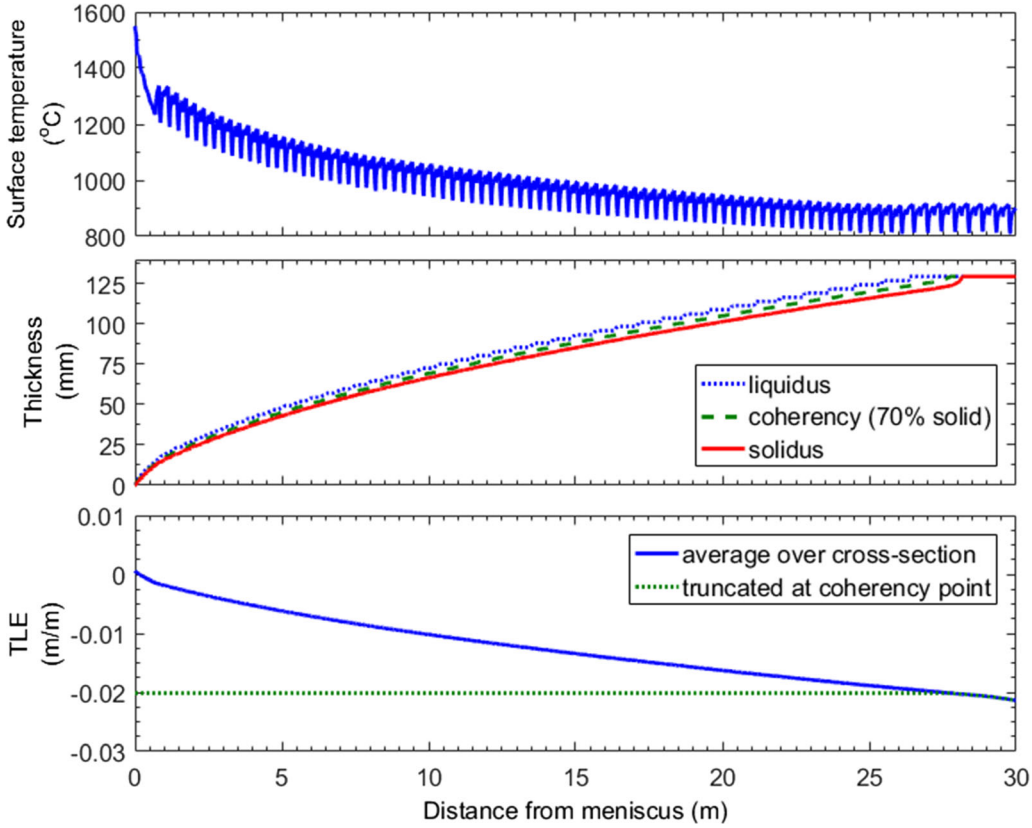

Fig. 6—Steady-state surface temperature, shell thickness, and average TLE profiles down the caster (AM caster at 1.1 m/min).

delay, the strain gauge measurements of roll force decrease when the casting speed decreases, which indicates that the liquid core has shrunk and is no longer beneath the measured support roll. When the speed rises again, there is a longer delay before the measurements increase back to their original values. Based on which roll forces are reading high and which are reading low, the metallurgical length can be localized to between two sets of instrumented rolls.

Figures 7(c) through (e) show predictions of CONOFFLINE for the speed change in Figure 7(a). The model produces a remarkable quantitative match in the time domain of the relative changes in the dynamic strain gauge measurements. Specifically, the predicted timing of changes in thermal linear expansion (TLE) in Figure 7(c) match very well with the timing of the changes in roll loads (microstrain) in Figure 7(b). After the speed drop, the metallurgical length decreases, and the roll loads decrease as the metallurgical length passes the roll. Since roll 79 is further down in the caster from the meniscus and is closet to metallurgical length before the speed drop, it is the first roll respond to change. The model also predicts the correct sequence of the time delays, and the predicted times of change are very close to the measurements. In Figure 7(c), the times with 0 TLE indicate the model predicts that the steel beneath that particular support roll is not yet coherent. Once it reaches coherency (assumed to be 70 pct), the figure shows the average TLE of the steel beneath the roll. Since the actual strain on the rolls depends on the difference between roll gap and thermal shrinkage, and the stiffness of the segment, this provides only a qualitative comparison to the strain measurements.

The model-predicted TLE shows a longer delay and a faster change during the speedup than during the slowdown, which agrees with the measurements. Following the slowdown in casting speed, the measured strain and model-predicted TLE both decrease. Then, as the casting speed resumes increasing, both the strain gauge measurements and model TLE predictions dip further before rebounding back up to a steady value.

An essential feature of the CONOFFLINE model ignoring axial conduction and simulating independent 1-D slices is that transient behavior can last no longer than one "dwell time" of the caster, *i.e.*, the time it takes for steel to travel from the meniscus to the caster exit. A previous model[6] which did include the effect of axial conduction, reported that transient effects after a slowdown took longer to settle than after a speedup, and exceeded the dwell time, suggesting that axial conduction may be significant. The current new results show that the timing of the measured transient response agrees with CONOFFLINE predictions, so the assumption of axial heat transfer dominated by advection is validated.

For further examination, Figure 7(e) shows the surface temperatures at important locations in the strand during these transient conditions. For reference, segment 13 contains the four instrumented rolls where the load was measured and TLE was predicted. The surface

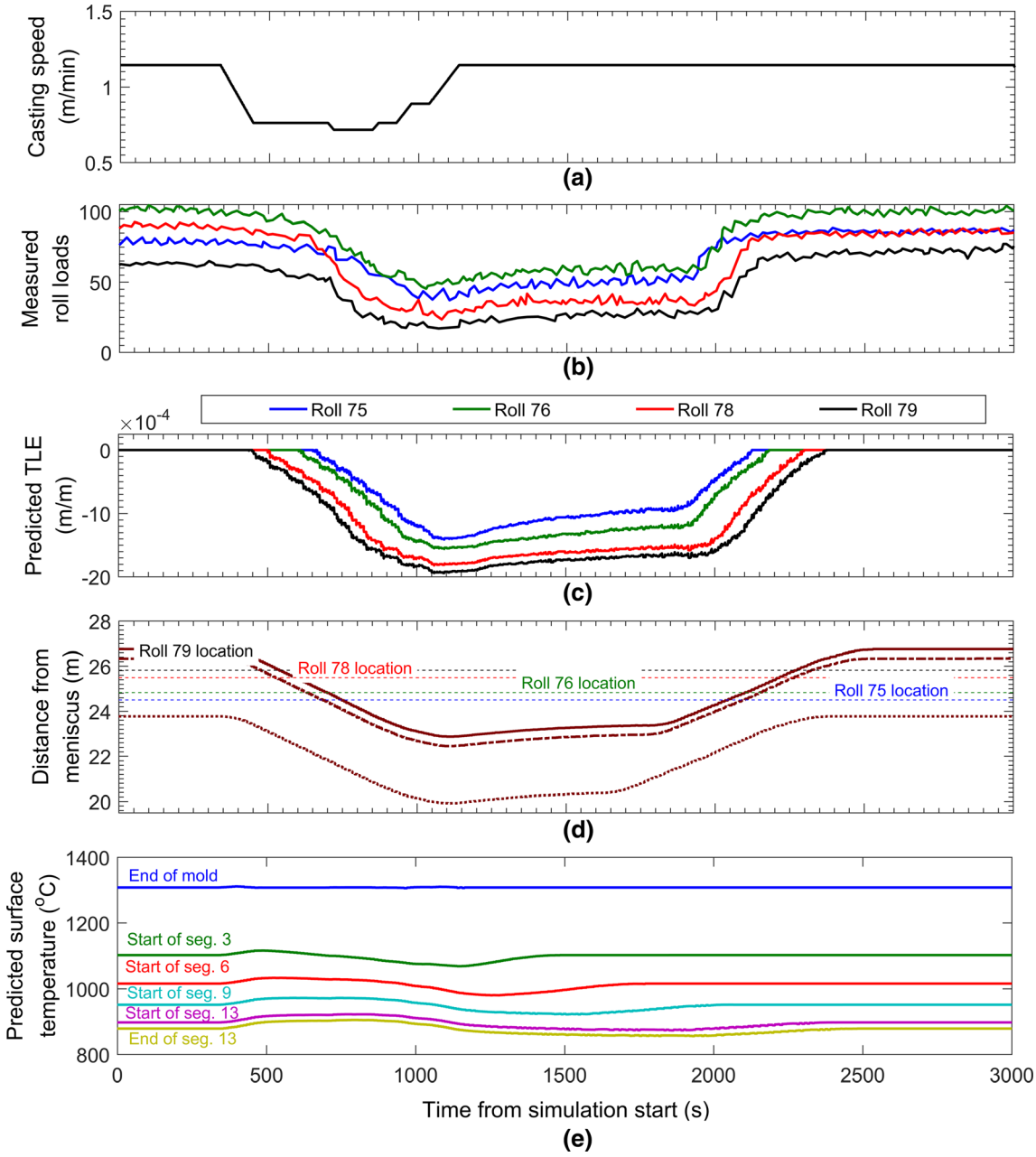

Fig. 7—(*a*) Casting speed during ArcelorMittal plant trial[24] (*b*) Strain gauge measurements collected from the ArcelorMittal plant trial[24] (*c*) CONOFFLINE model predictions of strand thermal shrinkage (*d*) CONOFFLINE model predictions of metallurgical length for different solidification fractions (*e*) CONOFFLINE model predictions of strand surface temperature history at selected locations.

temperature first increases after the speed drop, as the "spray table" control drops the cooling water flow rate immediately after the speed drop that makes the strand surface temporarily hotter. After the initial increase, the surface temperature gradually decreases, as the strand is moving slower giving more time for the strand to cool down. Therefore, the overall strand is growing colder, as can be seen in the metallurgical length or thermal shrinkage.

IV. CASE STUDIES

In the next two sections, the validated CONOFFLINE model is applied to explore dynamic thermal behavior of a thin-slab caster, similar to that at Nucor Steel in Decatur, AL. Specifically, the effect of sudden drops or increases in casting speed are investigated, starting from steady casting conditions in this commercial thin-slab caster.

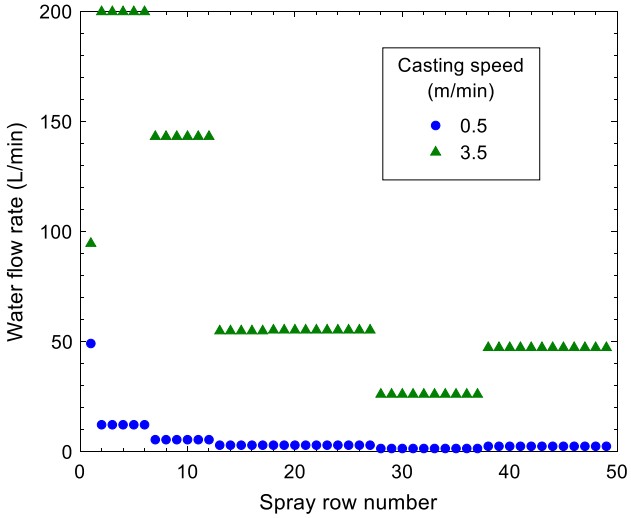

Fig. 8—Portion of "spray-table" of speed-based water flow rates (thin-slab caster).

Simulations are based on a thin-slab caster with strand thickness, L, of 90 mm.[13] for a typical low-carbon steel grade described in Section II. The mold heat flux in this caster was characterized by extensive plant measurements,[26]

$$\bar{q}_{\mathrm{m}}\left[\mathrm{MW/m^2}\right] = 1.197(v_{\mathrm{c}}[\mathrm{m/min}])^{0.544} \qquad [14]$$

Mold exit is at 0.85 m and the spray cooling region of the caster is 11.2 m long. Bending occurs from 1.6 to 2.5 m, and straightening happens from 6.7 to 8.5m down from the meniscus. Several different spray cooling control methods are evaluated. First, the spray water flow rates are kept constant, to investigate the dynamics of the heat transfer and solidification alone. Second, the spray water flow rates are chosen based on casting speed according to a spray table, which is typically used in practice. This is illustrated in Figure 8 for two of the casting speeds in the simulations below. Third, a proportional-integral controller is applied to maintain the surface temperature profile, as described in Reference 5.

V. RESULTS FOR CONSTANT COOLING (NO SPRAY CONTROL)

The most common casting speed for this commercial caster is 3.5 m/min, so that is chosen as the initial condition. At time $t = 0$, in each of the following simulations, the casting speed suddenly drops. The most severe speed drop that occurs in practice is in the case of a sticker (potential breakout) alarm, in which the casting speed suddenly drops to 0.5 m/min (in this particular case, a drop of 3 m/min). Therefore, this is the lowest casting speed considered.

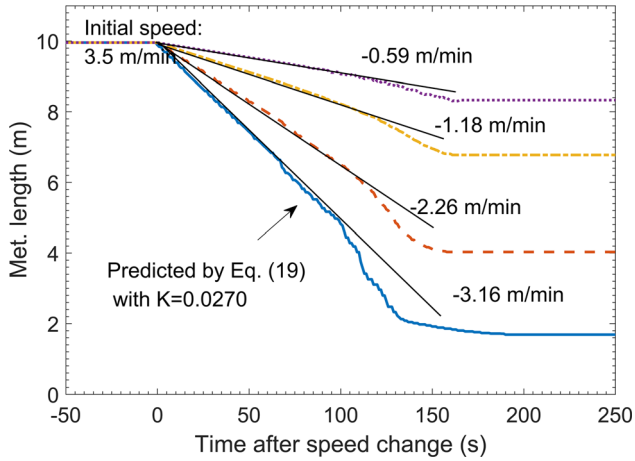

Fig. 9—Metallurgical length during sudden speed drops from 3.5 m/min.

For this set of "no-control" simulations, the secondary cooling sprays were left constant. The spray rates used are for the initial 3.5 m/min casting speed, given in Figure 8. Figure 9 illustrates casting speed drops of 0.5, 1, 2, and 3 m/min, respectively. Note that the temperatures take significantly longer to settle for the larger speed drops. The temperature settling time is the time needed for surface temperature to stay within 1 °C of its final value, and the metallurgical length settling time is the time needed to stay within 25 mm of the final metallurgical length.

Figure 9 compares the transient behavior of metallurgical length for the four different speed drops. The settling time is about 200 seconds, for all four metallurgical lengths. Interestingly, it decreases slightly with larger speed drops. For all cases, the decrease in metallurgical length is initially linear, with a slope that almost exactly matches the drop in casting speed. The slope then steepens before it finally gradually approaches the new steady-state length.

A. *Solidification Constants "K-factors"*

In fact, this transient behavior is expected, based on the simplest models of the solidifying steel shell growth used by caster engineers. Specifically, the shell thickness s at a distance z from the meniscus down the caster can be approximated by:

$$s = K\sqrt{\tau(z)} \qquad [15]$$

where $\tau(z)$ is the "dwell" time for a point on the steel strand to travel from the meniscus to distance z down the caster. K is the solidification coefficient, or "solidification rate constant," which depends on the strand thickness, L, the superheat, the chemical composition, and the surface cooling intensity. This dependence on the square root of time appears in analytical solutions to solidification PDEs with simplified boundary conditions.[32] When the casting speed is constant, Eq. [15] is simply

$$s = K\sqrt{\frac{z}{v_c}} \quad [16]$$

where v_c is the casting speed. Setting $s = L/2$, Eq. [16], can be solved for the metallurgical length at steady-state,

$$z_{ML} = \frac{L^2}{4K^2} v_c. \quad [17]$$

However, for a sudden drop in casting speed from v_{c_1} to v_{c_2} at time $t = 0$, $\tau(z,t)$ at any time during this transient process is:

$$\tau(z,t) = \begin{cases} \frac{z}{v_{c_1}}, & t < 0 \\ \frac{z}{v_{c_1}} + t\frac{v_{c_1} - v_{c_2}}{v_{c_1}}, & 0 < t < \frac{z}{v_{c_2}} \\ \frac{z}{v_{c_2}}, & \frac{z}{v_{c_2}} < t \end{cases} \quad [18]$$

Combining Eqs. [17] and [18], gives,

$$z_{ML}(t) = \begin{cases} \frac{L^2}{4K^2} v_{c_1}, & t < 0 \\ \frac{L^2}{4K^2} v_{c_1} + t(v_{c_1} - v_{c_2}), & 0 < t < \frac{L^2}{4K^2} \\ \frac{L^2}{4K^2} v_{c_2}, & \frac{L^2}{4K^2} < t \end{cases} \quad [19]$$

Thus, the *K*-factor model makes two important two predictions. Firstly, the metallurgical length should move at exactly the difference between the two casting speeds after a sudden speed change. As discussed above, this holds best shortly after the speed change. Secondly, the transient (settling time) in metallurgical length should take the same time for any given initial speed for the same final casting speed.

B. *Metallurgial Length Settling Times*

From Eq. [19] the settling time for metallurgical length can be estimated as follows:

$$t_{ML} = \frac{L^2}{4K^2} \quad [20]$$

Figure 9 compares the transient behavior of metallurgical length for the four different speed drops. The settling time is about 170 seconds, except for the 3 m/min speed drop case, which takes a little longer (about 200 seconds) for metallurgical length to reach steady state. For all cases, the decrease in metallurgical length is initially linear, with a slope that almost exactly matches the drop in casting speed. The slope then steepens before it finally gradually approaches the new steady-state length. The *K*-factor based on final solidification time is calculated for each of the steady metallurgical lengths and speeds in these simulations in Table I, based on a slab thickness of 90 mm (3.51 in). Note that the *K*-factor generally increases very slightly with decreasing casting speed, but is much smaller at 0.5 m/min. These differences are due to the secondary cooling practice. As illustrated in Figure 8, the spray cooling in the early segments of the caster are much higher than the spray rates lower in the caster. In these first several zones, where spray rates are high, shell growth is faster (*i.e.*, so *K*-factor is larger) which can be seen in Table II for all but the lowest casting speed (0.5 m/min). At that speed, the metallurgical length is small enough that mold heat flux is more important. As shown in Figure 10, the average temperature in the mold increases slightly due to the mold heat flux chosen in Eq. [14],[26] causing slower shell growth and a smaller K-factor. The *K*-factor according to different casting conditions, like casting speed and spray flow rates, however, for the cases, the settling time for sudden speed change can be estimated by choosing $K = 0.027$ m/min$^{0.5}$.

Figure 11 summarizes the settling times results from CONOFFLINE for the metallurgical length for both decreasing and increasing speed (described in detail in section V. D). These times should all be equal, according to Eq. [20]. The difference in settling times is due to the differences in spray cooling, which cause slight differences in *K*-factor. For example, decreasing *K*-factor from 0.0270 to 0.0256 (5 pct) causes an increase in settling time from 2.78 to 3.09 min (10 pct).

C. *Surface Temperature Settling Times*

The temperature settling time is the time needed for surface temperature to stay within 1 °C of its final value. While the metallurgical length settling time is relatively constant, the settling time for surface temperature increases in inverse proportion to casting speed. Surface temperatre settling times have an upper bound, t_{max}, that can be found by solving

$$z = \int_0^{t_{max}} v_c \, dt \quad [21]$$

where z is the distance of the particular location in the caster from the meniscus, and the speed change occurs at time $t = 0$. If the speed is constant after the initial change, Eq. [21] can be easily solved:

Table II. Calculated *K*-Factors for Thin-Slab Caster Based on Eq. [14] and Fig. 8 at 3.5 m/min

Casting Speed (m/min)	Steady-State ML (m)	Time from Meniscus to ML (min)	*K* (m/min$^{0.5}$)
3.5	9.955	2.844	0.0267
3	8.33	2.807	0.0269
2.5	6.775	2.777	0.0270
1.5	4.03	2.687	0.0275
0.5	1.685	3.370	0.0245

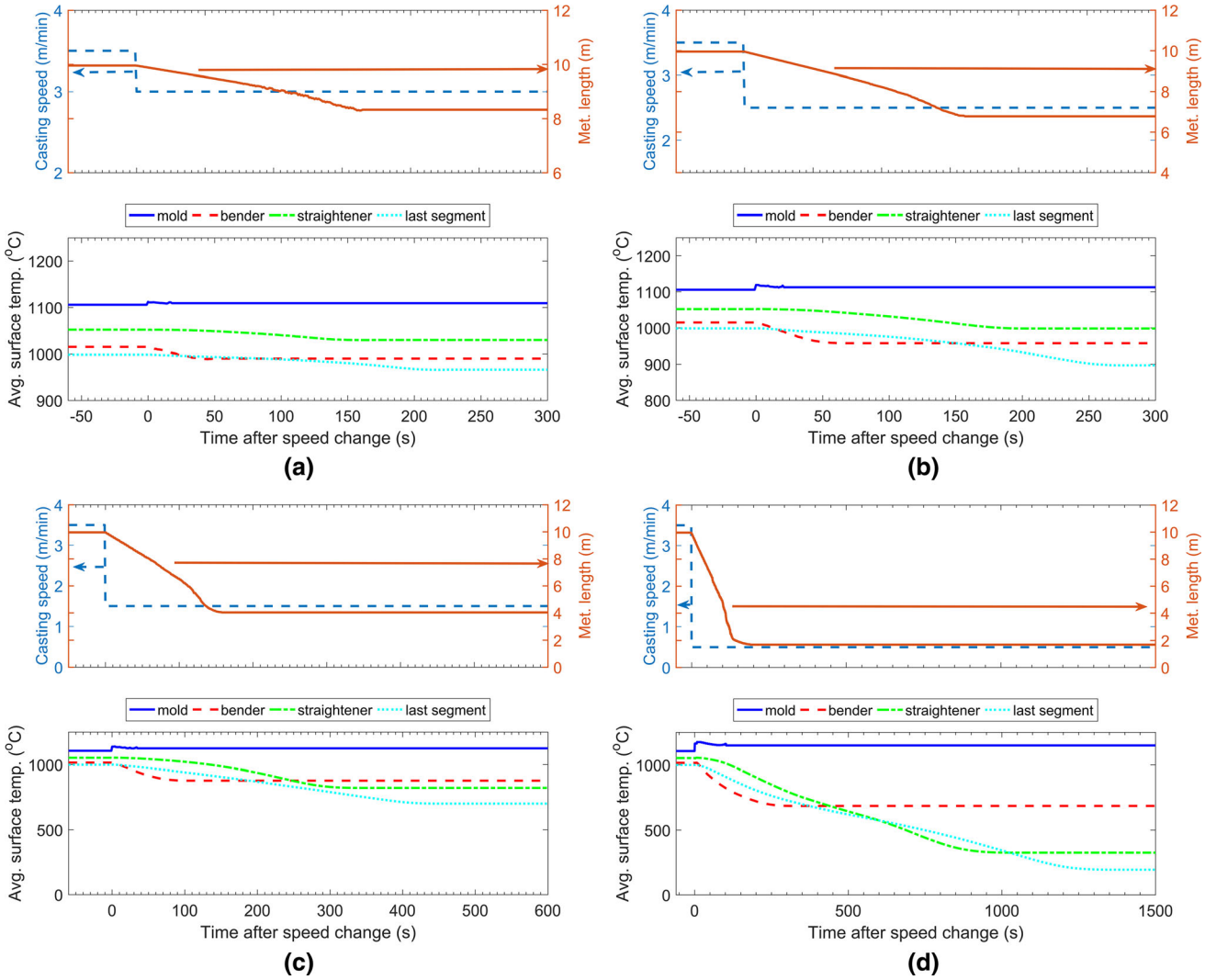

Fig. 10—Model prediction of thin-slab caster during sudden speed drops of (*a*) 0.5 m/min, (*b*) 1.0 m/min, (*c*) 2.0 m/min, and (*d*) 3.0 m/min.

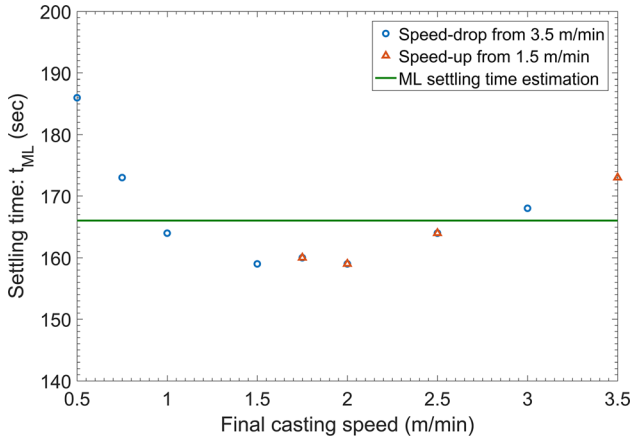

Fig. 11—Settling times for metallurgical length calculated from CONOFFLINE simulations compared with estimate, Eq. [19].

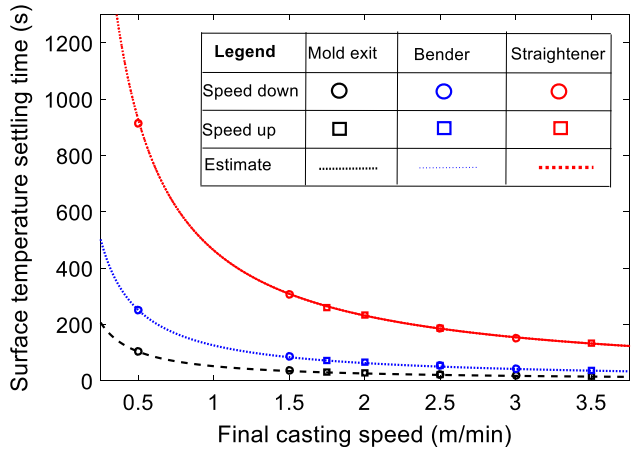

Fig. 12—Settling times for surface temperature in bender, straightener, and final segment, comparing results from CONOFFLINE with estimates using Eq. [21] (initial speeds of 1.5m/min for speedup and 3.5m/min for slowdown).

$$t_s \leq \frac{z}{v_{c,final}} \quad [22]$$

where $v_{c,final}$ is the speed after the speed change. Figure 12 shows the surface-temperature settling times results from CONOFFLINE, compared with estimates using Eq. [22] with an equality sign. As the figure shows, the estimate holds reasonably well for all of the simulations. With the two smaller speed drops, Figures 10(a) and (b), the temperature gradually lowers. It takes longer to change in the straightener and last segment because those segments, being further from the meniscus, have longer dwell times. In the Figure 10(d), there are inflection points in the temperatures in these latter two segments. The non-uniform spray cooling causes hotter internal temperatures, and also the reduced cooling rates at the surface seen in the figures.

D. *Effect of Speed Increases*

The previous sections have investigated the effect of casting speed drops, with results for 0.5, 1, 2, and 3 m/min drops shown in Figure 10. To investigate the effect of speed increases, 0.25, 0.5, 1.0, 2.0 m/min increases from 1.5 m/min initial casting speed were simulated. An example (2.0 m/min increase) is shown in Figure 13 as other cases had similar responses. Similar to when the caster slows down, the initial slope of the metallurgical length is approximately equal to the change in casting speed. Although not as obvious as in the speed drop cases, the rate of change of the metallurgical length does increase slightly as time progresses.

Figure 14 shows the changing metallurgical lengths for these cases. In each case, the metallurgical length reaches its steady value in approximately the same time, about 160 seconds. Compared to the speed drop cases where speed dropped, shown in Figure 9, the rate of increase of the metallurgical length remains more constant with speed increases. This is because as shown in Figure 8, the flow rates are smaller further down the caster, and the lower cooling rate in the last spray zones has less effect on the overall K-constant. The actual rates are close to those predicted with Eq. [20].

E. *Effect of Complex Speed Changes*

This subsection examines the transient response to complex speed changes for the thin-slab caster with constant spray water flow rates. The response is complicated when the casting speed changes again before allowing the strand to reach steady state after the previous speed change. Simulations were conducted for casting speed drops from 3.5 to 2.5 m/min and then increases back to 3.5 m/min, with different times between the two speed changes.

Figure 15(a) shows the transient response with 300 seconds between speed changes. In this case, the metallurgical length and surface temperature simply change from one steady state to another, and the results up to 300 seconds match those in Figure 10(b). This is because the spray cooling region of the caster is 11.2 m long, so at 2.5 m/min it takes only about 4.5 min (270 seconds) for the first speed change to complete.

However, Figure 15(b) shows results for a shorter time, 180 seconds, between the speed changes, which is not enough to reach the steady state, so the natural behaviors discussed so far in this paper are interrupted. In this, the temperature in the last segment continues to decrease after the speed increases. Here two conflicting transient effects are spotted: the speedup naturally causes the steel temperature to increase, but the previous slowdown created a large amount of cooler steel which continues to move through the caster and tends to decrease temperature. The net result for this case is initially to decrease surface temperature after the speed increases. Eventually, the temperature increases, after a delay time, which increases with distance down the caster. Thus, the surface temperature increases after a delay after the speed increase, the further down the caster the larger the delay. In Figure 15(c), in which only 60 seconds passes before the speed increase, the conflicting transient trends affect the metallurgical length as

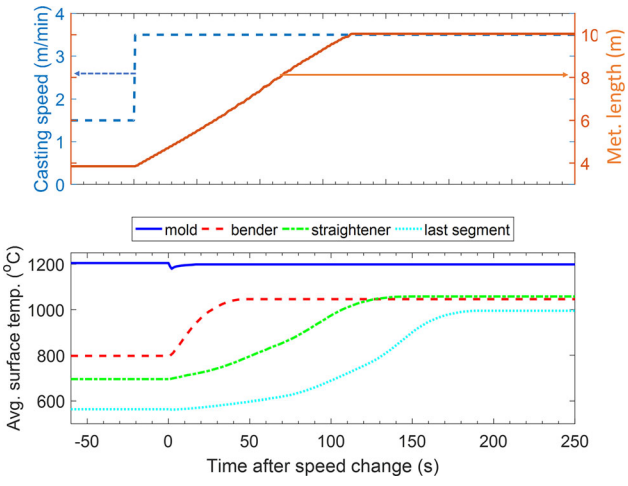

Fig. 13—Surface temperature and metallurgical length increases after sudden 2 m/min speed increase (from 1.5 to 3.5 m/min in thin-slab caster).

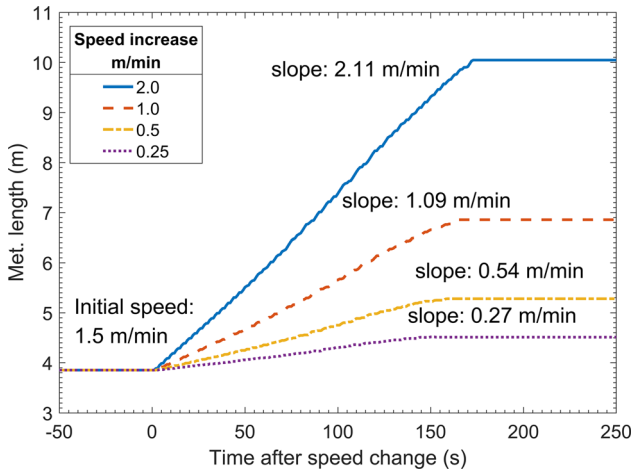

Fig. 14—Metallurgical length response after sudden speed increases from 1.5 m/min.

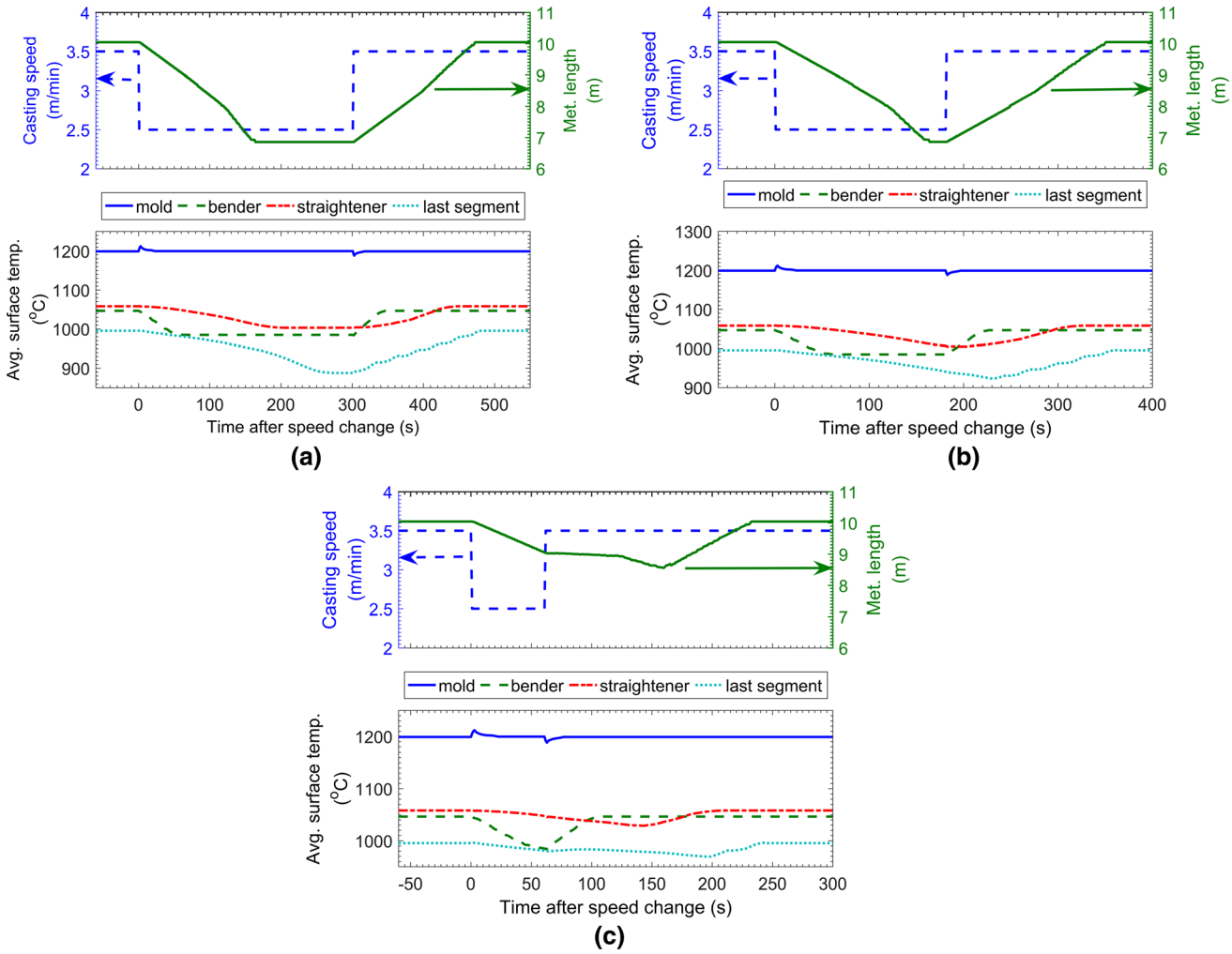

Fig. 15—Model prediction of thin-slab caster during a sudden speed drop of 1 m/min, followed by a corresponding increase, (constant spray cooling), with times between speed changes of: (*a*) 5 min, (*b*) 3 min, and (*c*) 1 min.

well. Specifically, the metallurgical length stops decreasing right after the speed increase, then decreases for a while, before finally increasing to steady state.

VI. EFFECT OF SPRAY COOLING CONTROL

The constant spray cooling practice investigated in Section V is not practiced in the steel industry. Instead, the spray water flow rates adjust according to changing casting speed. This section investigates transient thermal behavior for two popular spray cooling methods: spray table control and PI control.

Figures 16(a) and (b) present results for two cases using the "spray-table" open-loop control method. With this method, the spray rates are chosen based only on the current casting speed, as shown in Figure 9. Thus, water flow rates decrease simultaneously everwhere in the caster, at the same instant that the speed decreases. Thus, the surface temperatures everywhere inside the caster (especially the bender and straightener) overshoot before coming back to steady-state. The sprays change immediately when the speed changes, and do not account for the dwell time of the material in the caster. For the same reason, the metallurgical length has inflection points both during the slowdown and speedup. In Figure 16(a), the speed drop lasts for 300 seconds, which allows the caster to reach a new steady state. However, the surface temperatures are higher at some locations at the lower speed, even at steady state. This is because the spray rates were not exactly tuned to ensure constant temperatures at all casting speeds. When there is not enough time for the steel to reach steady-state before the second speed change, the different transient beahviors due to the speed change and due to the spray changes overlap. Thus, in Figure 16(b), with only 60 seconds between speed changes, the overlapping transients cause complex behavior in the metallurgical length and temperature evolution.

Figures 16(c) and (d) show the same two casting speed cases but using a Proportiaonal-Integral (PI) controller that aims to keep surface temperature constant during the speed change.[5] With this controller, flow rates are changed according to the difference between average surface temperature in each spray cooling zone based on proportional gains that were optimized in previous work, and an anti-windup algorithm to avoid instabilities.[5] As

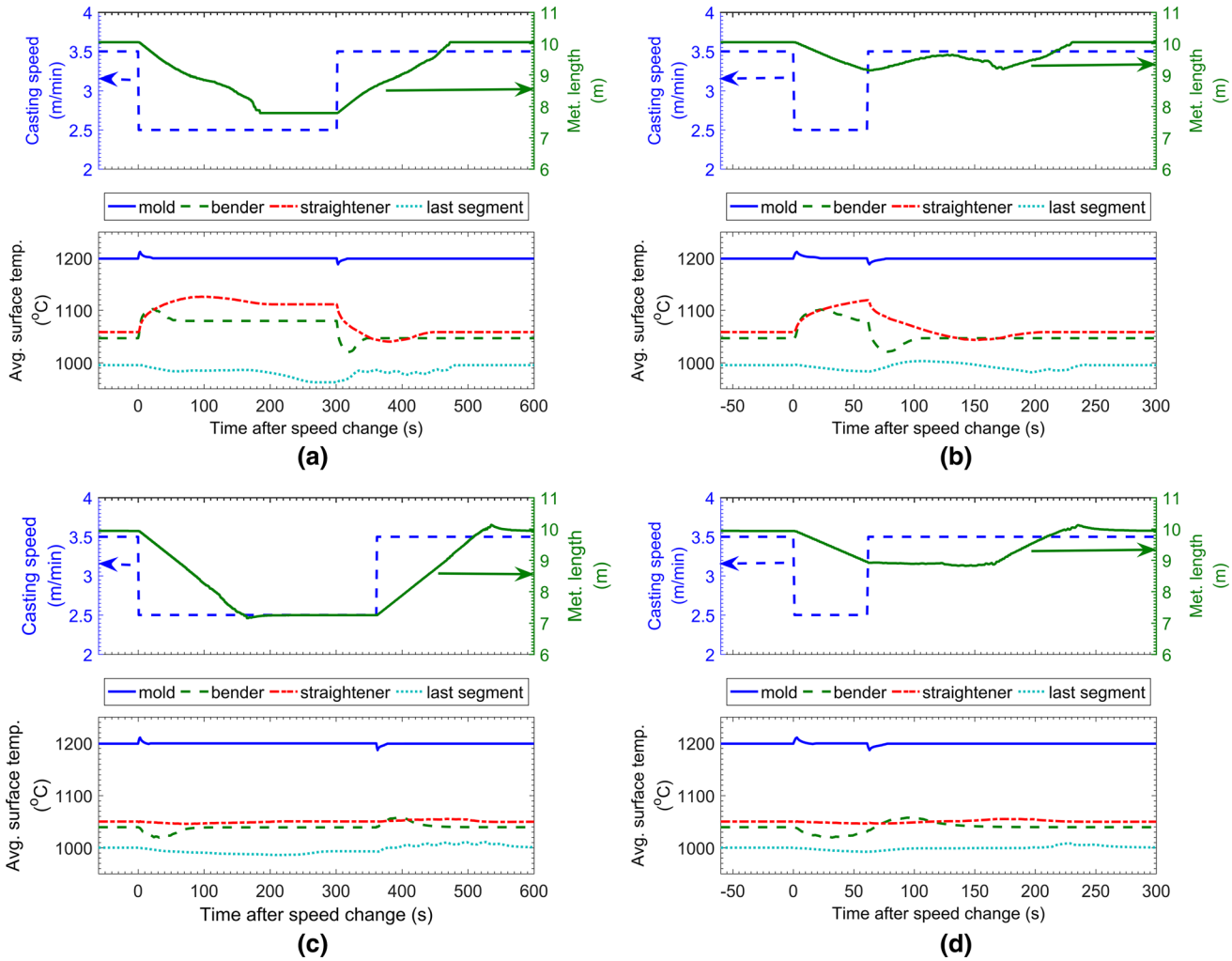

Fig. 16—Model prediction of thin-slab caster during speed dips with different spray cooling control methods, (*a*) 5 min between speed changes, spray table cooling control, (*b*) 1 min between speed changes, spray table cooling control, (*c*) 5 min between speed changes, PI cooling ontrol, and (*d*) 1 min between speed changes, PI cooling control.

shown in Figure 16(c), the PI controller achieves much more consistent surface temperatures throughout the transitions between slowdown and speedup. Metallurgical length evolves almost linearly between the steady-state conditions. Tracking is not perfect, however, as the metallurgical length undershoots its final value on the slowdown, and overshoots on the speedup. This illustrates the trade-off between temperature tracking and metallurgical length tracking goals. The serious danger of surface temperature PI control for the sudden speedup case is that this resulting overshoot could cause a whale to form after the speedup for this case, if the metallurgical length was already very near to caster exit. However, this PI controller responds directly to the heat transfer dynamics of the steel regarding surface temperature. Thus, even for the highly-transient situation with only 60 seconds between speed changes, the PI controller is equally good at maintaining constant surface temperature during the transition, as seen in Figure 16(d).

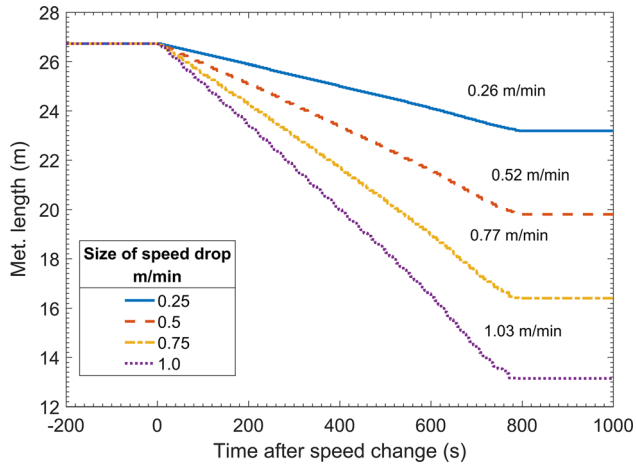

Fig. 17—Metallurgical length in thick-slab caster during sudden speed drops from 2.0 m/min.

Table III. Calculated *K*-Factors for Thick-Slab Caster

Casting Speed (m/min)	Steady-State ML (m)	Time from Meniscus to ML (min)	*K* (m/min$^{0.5}$)
2.0	26.72	13.36	0.0300
1.75	23.19	13.25	0.0302
1.5	19.81	13.21	0.0303
1.25	16.41	13.13	0.0304
1.0	13.14	13.14	0.0303

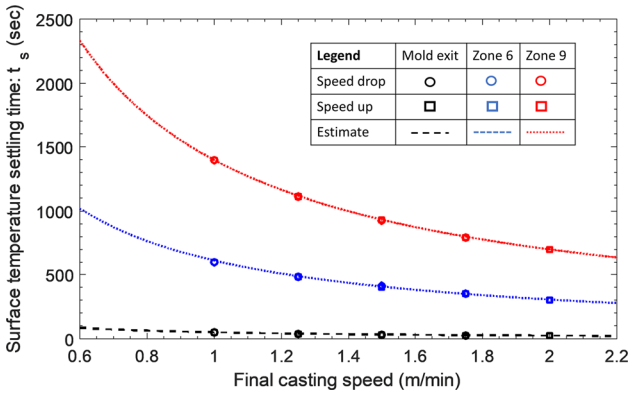

Fig. 18—Settling times for surface temperature at exit of different zones down the thick-slab caster, comparing results from CONOFFLINE for different speedup and slowdown cases with estimates using Eq. [22] (initial speeds of 1.0 m/min for speedup and 2.0 m/min for slowdown).

VII. EFFECT OF STRAND THICKNESS

This section explores the effect of slab thickness on the metallurgical length and surface temperature settling time relations by investigating a typical thick-slab caster for similar scenarios of sudden speed drops and increases. Simulations are based on a 221 mm thick-slab caster[7] for the same 0.05 wt pct low-carbon steel grade studied in the previous sections. For this caster, mold exit is located at 0.86 m, zone 6 ends at 10.2 m, and zone 9 ends at 23.3 m from the meniscus. The average heat flux in the mold was found using Eq. [10] of Reference 7. For secondary cooling, the spray water flow rates are kept constant (no control) to investigate the dynamics of the heat transfer and solidification alone. Details of the casting conditions can be found in Table II of Reference 7. Casting speeds of 1.0 and 2.0 m/min were chosen as the initial casting speed for speed increases and speed drops respectively.

Figure 17 shows the effect of casting speed change on the evolution of the metallurgical length for speed drops of 0.25, 0.5, 0.75, and 1.0 m/min. The decrease is almost exactly linear and the calculated initial slopes of these lines (0 to 60 seconds, as indicated on the figure) match the drop in casting speed within 5 pct. The transient behavior of metallurgical length for these four casting speed drops is similar to that of the thin-slab caster. For the same speed drop, it takes longer for the thick-slab caster to settle than the thin-slab caster, because the greater thickness contributes to longer times. This is because the *K*-factor is 10 pct larger than found in the thin-slab caster, due to the different water flow rates. The metallurgical-length settling times for the different speed changes are all very close at about 10 s, which is estimated reasonably well by Eq. [20] with a *K*-factor of 0.0303 m/min$^{0.5}$. The *K*-factors are very similar for all 4 cases, as listed in Table III.

The settling time results for surface temperature for these 8 cases (4 speedup and 4 slowdown) are shown in Figure 18. Estimates using Eq. [20] are also shown in this figure. As expected, the times are much longer compared to the thin-slab caster, due to the lower casting speeds involved. According to the estimates from Eq. [20], the settling time depends only on final casting speed and location, for a given *K*-factor. Thicker slabs have slightly longer settling times, at a given distance, because the interior takes longer to reach steady state, and this has a small effect on surface temp. Finally, the surface-temperature settling times are very similar for speed increases and decreases, even for different magnitudes of speed change, owing to the constant spray cooling conditions (and constant *K*-factor) in this caster.

VIII. CONCLUSIONS

The real-time model, CONONLINE, which simulates heat transfer in a 2-D longitudinal plane down a continuous steel slab caster by interpolating multiple 1-D moving slices, was modified into the offline modeling tool, CONOFFLINE, to investigate transient thermal behavior in typical commercial slab casters. The model was validated by comparing model predictions of thermal linear expansion through the strand thickness with transient measurements of roll forces in a thick-slab caster during a series of speed changes. The predicted timing of the transient behavior matches closely to that of the measurements, in many different respects. This suggests that the model formulation, including its assumption of negligible axial heat conduction, is valid in real casters for actual casting conditions.

The settling time for metallurgical length to stabilize to the new steady state after a sudden speed change depends on the time needed for new steel at the meniscus to move down the caster to the location in the caster where the new metallurgical length is found. A simple equation based on *K*-factor is derived to estimate the

settling time for metallurgical length for a single speed drop, and matches reasonably well with the simulation results.

The surface temperature takes longer to stabilize during casting-speed transients. The settling time for surface temperature can be estimated by Eq. [21], which is the dwell time of the steel to move to a specific location. Therefore, only final casting speed matters, and this settling time increases with decreasing speed.

PI control of surface temperature performs much better than "spray table" control, in maintaining surface temperature during a complex speed change, such as a sudden slowdown followed quickly by a speedup back to the original casting speed. When moving from one steady-state to another, the metallurgical length moves almost linearly with time, especially with PI control. The trends of transient behavior are similar for thin- and thick-slab casters.

Increasing strand thickness tends to increase both settling times, owing to the longer times and distances taken to replenish the steel in the entire liquid pool, which affects both ML and surface temperature. Because thick-slab casters typically have slower casting speeds than thin-slab casters, it takes longer to settle with increased thickness, owing to the longer times for steel to pass through the caster.

ACKNOWLEDGMENTS

The authors are grateful for support of this work by the member companies of the Continuous Casting Center at Colorado School of Mines, the Continuous Casting Consortium at University of Illinois at Urbana-Champaign, and the National Science Foundation GOALI program (Grant No. CMMI 1300907).

NOMENCLATURE

c_p	Nominal specific heat
c_p^*	Effective specific heat, including effect of latent heat
f_p	Mass fraction of phase p = α, γ, δ, s, l (respectively, α-ferrite, austenite, δ-ferrite, solid, and liquid)
$f_{s,cohere}$	Minimum solid fraction necessary for strand to be coherent
h_{sw}	Heat transfer coefficient due to spray cooling
i	Used for numbering CON1D slices in CONOFFLINE
K	"K-factor" in simple model of shell growth
k	Thermal conductivity
L	Thickness of the strand (in the x-direction)
L_f	Latent heat of solidification
$L(T)$	Length of a temperature dependent material at temperature T
$\Delta L(T)$	Change in length of a temperature dependent material from temperature T_{ref} to temperature T
L_x	Characteristic length in x-direction
L_z	Characteristic length in z-direction
Pe	Péclet number
Q_{sw}	Spray water flux (volume of water hitting strand surface per unit area and time)
$\bar{q}_m$	Average heat flux in the mold
q_{sw}	Heat flux due to spray cooling
s	Shell thickness
T	Temperature
$\hat{T}$	Strand temperature predicted by CONOFFLINE
T_i	Temperature of CON1D slice number i
TLE	Thermal linear expansion
T_{ref}	Reference temperature used in calculation of TLE
T_{surf}	Temperature of strand surface
T_{sw}	Temperature of spray cooling water
t	Time
t_i^0	Time when CON1D slice number i is at the meniscus
t_{max}	Estimated upper bound on temperature settling time
v_c	Casting speed
v_{c_1}	Casting speed before a sudden speed change
v_{c_2}	Casting speed after a sudden speed change
$v_{c,final}$	Casting speed at the end of a speed change
x	Distance from inner radius surface
z	Distance from meniscus
z_{cohere}	Distance from meniscus where strand is fully coherent
z_i	Distance from meniscus of CON1D slice number i
z_{ML}	Metallurgical length
ρ	Density
ρ_{ref}	Density at reference temperature, used to calculate TLE
$\rho(z)$	Average density of strand at distance z from the meniscus
τ	Steel dwell time in the caster

REFERENCES

1. J. Sengupta, M.-K. Trinh, D. Currey, and B.G. Thomas: *AISTech - Iron and Steel Technology Conference Proceedings*, AIST, Warrendale, PA, 2009, pp. 1177–86.
2. M. Miyazaki, K. Isobe, and T. Murao: *Nippon Steel Tech. Rep.*, 2013, vol. 104, pp. 48–53.
3. C.H. Yim, J.K. Park, B.D. You, and S.M. Yang: *ISIJ Int.*, 1996, vol. 36 (Supplement), pp. S231–34.
4. A. Ghosh: *Sadhana*, 2001, vol. 26 (1–2), pp. 5–24.
5. B. Petrus, K. Zheng, X. Zhou, B.G. Thomas, and J. Bentsman: *Metall. Mater. Trans. B*, 2011, vol. 42 (1), pp. 87–103.
6. R.A. Hardin, K. Liu, C. Beckermann, and A. Kapoor: *Metall. Mater. Trans. B*, 2003, vol. 34 (3), pp. 297–306.
7. Z. Chen, J. Bentsman, B.G. Thomas, and A. Matsui: *Iron Steel Technol.*, 2017, vol. 14 (10), pp. 92–103.
8. Z. Chen, W. Drennan, B.G. Thomas, J. Bentsman, and B.G. Thomas: in *2019 AISTech - Iron and Steel Technology Conference Proceedings*, AIST, Warrendale, PA, 2019, pp. 2075–84.
9. B. Petrus: PhD Thesis, University of Illinois at Urbana-Champaign, 2014.
10. J.K. Brimacombe and K. Sorimachi: *Metall. Trans. B*, 1977, vol. 8 (2), pp. 489–505.
11. A. Scholes, B. Patrick, and B. Barber: *Ironmak. Steelmak.*, 2005, vol. 32 (2), pp. 101–08.

12. Z. Chen, H. Olia, B. Petrus, M. Rembold, J. Bentsman, and B.G. Thomas: in *Materials Processing Fundamentals 2019, The Minerals, Metals &Materials Series*, 2019, pp. 23–35.
13. B. Petrus, D. Harnmon, M. Miller, B. Williams, A. Zewe, Z. Chen, J. Bentsman, B.G. Thomas, D. Hammon, M. Miller, B. Williams, A. Zewe, Z. Chen, J. Bentsman, and B.G. Thomas: *Iron Steel Technol*., 2015, vol. 12 (12), pp. 58–66.
14. E. Mizikar: *Trans. Metall. Soc. AIME*., 1967, vol. 239 (11), pp. 1747–53.
15. J. Lait, J. Brimacombe, and F. Weinberg: *Ironmak. Steelmak*., 1974, vol. 1 (2), pp. 90–97.
16. H. Shen, R.A. Hardin, R. Maenzie, and C. Beckermann: *J. Mater. Sci. Technol*., 2002, vol. 18 (4), pp. 311–14.
17. L.C. Hibbeler, K. Xu, B.G. Thomas, S. Koric, and C. Spangler: *Iron Steel Technol*., 2009, vol. 6 (7), pp. 60–73.
18. Y.A. Meng and B.G. Thomas: *Metall. Mater. Trans. B*, 2003, vol. 34 (5), pp. 685–705.
19. S. Louhenkilpi, E. Laitinen, and R. Nieminen: *Metall. Mater. Trans. B*, 1993, vol. 24 (4), pp. 685–93.
20. T. Räisänen, S. Louhenkilpi, T. Hätönen, J. Toivanen, J. Laine, and M. Kekäläinen: in *European Congress on Computational Methods in Applied Sciences and Engineering*, 2004, pp. 1–11.
21. S. Louhenkilpi, M. Mäkinen, S. Vapalahti, T. Räisänen, and J. Laine: *Mater. Sci. Eng. A*, 2005, vols. 413–414, pp. 135–38.
22. J. Ma, Z. Xie, and G. Jia: *ISIJ Int*., 2008, vol. 48 (12), pp. 1722–27.
23. B. Petrus, Z. Chen, J. Bentsman, and B.G. Thomas: *IEEE Trans. Automat. Contr*., 2018, vol. 63 (4), pp. 1090–96.
24. N. Gregurich, G. Flick, R. Moravec, and K. Blazek: *Iron Steel Technol*., 2012, vol. 9 (12), p. 62.
25. Y.M. Won, H.N. Han, T. Yeo, and K.H. Oh: *ISIJ Int*., 2008, vol. 40 (2), pp. 129–36.
26. P. Duvvuri, B. Petrus, and B.G. Thomas: *AISTech - Iron and Steel Technology Conference Proceedings*, AIST, Warrendale, PA, 2014, pp. 2881–93.
27. T. Nozaki, J. Matsuno, K. Murata, H. Ooi, and M. Kodama: *Trans. Iron Steel Inst. Jpn*., 1978, vol. 18 (6), pp. 330–38.
28. G.F. Franklin, J.D. Powell, and M.L. Workman: *Digital Control of Dynamic Systems*, Addison-Wesley, Boston, 1997.
29. K. Harste: Doctoral dissertation, Technical University of Clausthal, 1989.
30. A. Jablonka, K. Harste, and K. Schwerdtfeger: *Steel Res. Int*., 1991, vol. 62 (1), pp. 24–33.
31. I. Jimbo and A.W. Cramb: *Metall. Trans. B*, 1993, vol. 24 (1), pp. 5–10.
32. J.A. Dantzig and C.L. Tucker: *Modeling in Materials Processing*, Cambridge University Press, New York, 2001.
33. C. Cicutti, M. Valdez, T. Perez, G. Gresia, W. Balante, and J. Petroni: in *Proceedings of the 85th Steelmaking Conference*, Iron & Steel Soc., Warrendale, PA, 2002, pp. 97–107.
34. B.G. Thomas: in *Modeling for Casting and Solidification Processing*, Kuang-Oscar Yu, ed., CRC Press, New York, 2001, Ch. 15, pp. 499–540.